High local ionization density effects in x-ray excitations deduced from optical stimulation of trapped charge in Al_2O_3:C

2007 J. Phys.: Condens. Matter 19 116201

(http://iopscience.iop.org/0953-8984/19/11/116201)

IOP PUBLISHING JOURNAL OF PHYSICS: CONDENSED MATTER

J. Phys.: Condens. Matter **19** (2007) 116201 (15pp) doi:10.1088/0953-8984/19/11/116201

High local ionization density effects in x-ray excitations deduced from optical stimulation of trapped charge in Al_2O_3:C

M Jain[1], **L Bøtter-Jensen and K J Thomsen**

Radiation Research Department, Risø National Laboratory, Technical University of Denmark, DK-4000 Roskilde, Denmark

E-mail: mayank.jain@risoe.dk

Received 14 August 2006, in final form 31 January 2007
Published 27 February 2007
Online at stacks.iop.org/JPhysCM/19/116201

Abstract

X-rays are used extensively in luminescence studies. Recent studies have shown a strong sample and material dependence in the response of the optically stimulated luminescence (OSL) signal to x-rays, which cannot be accounted for by differences in the photoelectric cross-sections of these materials. In this paper we give direct experimental evidence for a high local ionization density caused during low energy x-ray interactions; this is similar to the effect produced by high LET (linear energy transfer) radiations such as protons. This effect is deduced on the basis of optical stimulation of trapped charge in carbon doped aluminium oxide (Al_2O_3:C) after exposure to different radiations (^{90}Sr/^{90}Y beta, proton, ^{137}Cs gamma and x-rays), and making a comparative analysis of the changes in the initial OSL decay rates. The sensitive parameter λ (the decay constant) is $>100\%$ larger for irradiations carried out with x-rays in comparison to that for low LET radiation such as beta particles.

We further show that the nature of the increase in λ with dose, $\lambda(D)$, is a saturating exponential function plus a constant (λ_0), and that both $\lambda(D)$ and λ_0 are unique for a given radiation type or more specifically its LET. Such behaviour is explained by superimposition of OSL from several first-order traps or by the presence of a competing trap in Al_2O_3:C. The understanding of x-ray interaction with OSL traps presented here explains the x-ray dose rate calibration problem in different materials, and opens up the area of studying ionization density effects in low energy x-ray interactions using the OSL of Al_2O_3:C.

1. Introduction

Excitation of crystals with ionizing radiation creates electron–hole pairs in the valence band. Some of these electrons and holes are subsequently transferred via the delocalized bands to

[1] Author to whom any correspondence should be addressed.

localized states due to defects known as traps or centres. A later release of trapped charge by heat or light causes electron–hole recombination, and the resulting luminescence emission is a function of the energy absorbed per unit mass, also known as dose (unit Gy), during the initial excitation. Depending on the mechanism of charge release the process is called either thermoluminescence (TL) or optically stimulated luminescence (OSL). Both TL and OSL techniques are commonly used for dose determination in wide ranging applications such as environmental, accident, medical and space dosimetry where the excitation energy can be photons such as x-rays and gamma rays (e.g. medical scans and treatments), charged particles (e.g. space dosimetry, tumour therapy) or radiogenic emissions such as alpha, beta and gamma radiations (e.g. natural environment). In recent years a great interest has developed in *in vivo* measurement of x-ray doses using OSL detectors such as Al_2O_3:C during radiotherapy or diagnosis [1, 2].

It is often the case that dose calibrations are transferred from one radiation type to another with the underlying assumption that the luminescence efficiency is near identical for all radiation types having a low linear energy transfer (LET), e.g. photons and electrons. X-rays, in particular, have been used extensively in luminescence based dosimetric studies for almost two decades [3–7]. The widespread use of x-rays has primarily been because of its low LET, and because of the possibility it offers to select from a range of excitation energies. Moreover conventional x-ray sources (tubes) are radiationless when not operated (in contrast to radioactive sources), offer high dynamic range in dose rates, irradiate the sample area uniformly, and can be easily transported for mobile end-use measurements [8–10]. The easy mobility and control offers the potential for remote luminescence dosimetric measurements in space [11, 12].

Despite this widespread use and potential application the response of the OSL signal to x-rays remains poorly investigated. Recently, it has been shown that for a 50 kV x-ray tube the dose calibrations are strongly sample and material dependent [10, 12]. Thomsen *et al* [10] found that the observed sample dependence in quartz can be minimized by using a 200 μm Al absorber in front of the x-ray tube. The material dependence observed by Jain *et al* [12] was, however, much greater and cannot be eliminated by simple filtration. In sharp contrast to OSL, the response of TL to x-rays has been investigated in detail. Several studies have examined TL of lithium fluoride (LiF) after x-ray irradiation [13–19], and it has been shown that the nature of TL response is dependent on the presence of impurities such as Mg, Ti or Mg, Cu, P (e.g. [14, 15]). For example, it has been observed that at 30 keV there is about +30% and +10% change in TL efficiency in LiF:Mg, Ti and LiF:Mg, Cu, P, respectively. However, at 100 keV these efficiencies reduce to +10 and −20% [14, 16]. In addition to TL of LiF, changes in TL sensitivity of several other dosimeters such as $Li_2B_4O_7$, BeO, $CaSO_4$:Dy have also been reported ([17] and references therein). Horowitz and Olko [14] developed a microdosimetric target theory to explain efficiency changes in LiF. Similarly, Olko *et al* [16, 18, 19] have tried to explain the response of LiF to photon irradiation using the one hit detector model or the microdosimetric model of Geiß *et al* [20] developed originally for heavy charged particles ($Z \geqslant 2$). These models assume that the sensitivity change in TL from LiF occurs because of an increase in the microscopic dose. Apart from these various studies on TL signal, especially on the TL sensitivity in LiF (which has been investigated in great detail), there exists little experimental demonstration of the relationship between x-ray excitation and the response of luminescence traps and centres in a crystal. In particular, the effect of x-rays on the OSL traps has not been investigated to date. Considering the widespread use of x-rays and the great potential of remote and *in vivo* OSL dosimetry [12, 21], it becomes imperative that OSL–x-ray interactions are understood in detail.

In the following sections we present experimental evidence towards understanding these interactions. This is achieved by comparative analysis of changes in the decay rate of the initial OSL (first 2 s) in aluminium oxide, Al_2O_3:C (TLD 500) [22] after exposure to different kinds of radiations (beta, proton and x-rays). The proposed model for x-ray interactions in luminescence dosimeters is then tested on three different materials namely quartz, feldspar and Al_2O_3:C. Finally, the results are discussed for potential application of Al_2O_3:C to determine a radiation's LET at the target. It is concluded that the OSL signal of Al_2O_3 has a great potential for understanding radiation interactions at the micrometre and nanometre scales.

2. Experimental details

All OSL measurements were made using a Risø TL/OSL reader (TL/OSL-DA-15) [23]. This reader is equipped with a blue light stimulation unit for OSL (LEDs emitting at 470 ± 30 nm, $\sim$50 mW cm^{-2}), a heater plate underneath the sample, a 40 mCi beta (^{90}Sr/^{90}Y) source, and a photon counting system consisting of a 7.5 mm Hoya U-340 filter in front of a bialkali photomultiplier tube (Electron Tubes Ltd 9235 QA). For x-ray irradiations we used a Varian VF-50J x-ray tube (50 kV; 1 mA; 50 W) with tungsten target and a 4–50 kV DC Spellman high voltage power supply (XRM50P50X2666) [8]. The tube has integral shielding (provided by the manufacturer) and the beam is emitted through a 76 μm thick, 8 mm diameter beryllium window. The energy spectrum of the x-rays consists of bremsstrahlung and characteristic L-shell x-rays at about 9 keV. The mean energy for the unfiltered spectrum is about 19 keV for a potential of 40 kV. The tube is mounted on a brass collimator (length 35 mm) with a 200 μm thick aluminium end-window (diameter 10 mm) attached to the Risø TL/OSL reader.

In addition to x-rays various other types of radiation were used for comparison of the OSL responses. These were (a) a monoenergetic 662 keV gamma beam obtained from a ^{137}Cs point source at a distance of 2 m from the sample, (b) a 40 mCi ^{90}Sr/^{90}Y beta source ($\overline{E} \approx 600$ keV) mounted on the TL/OSL reader itself, and (c) A 60 MeV proton beam (at Paul Scherrer Institute, Switzerland) degraded using Al shields to achieve different proton beams from 60 to 11 MeV. The dose rate of the ^{90}Sr/^{90}Y beta source was determined for each sample by comparing the signal induced by a well known gamma dose (delivered by ^{137}Cs point source) to the signal induced by the ^{90}Sr/^{90}Y beta source. The same approach was used to determine the x-ray dose rates in the samples by comparison with the ^{90}Sr/^{90}Y beta source. The x-ray dose rates were further determined by using radiation sensitive GAF (gafchromatic EDT dosimetric) films. The proton dose rates at each energy were determined using ionization chambers.

The dosimeters used in this study were single crystal Al_2O_3:C pellets ($\varnothing = 5$ mm, $d = 1$ mm) doped with about 5000 ppm of carbon (TLD 500) [20], and natural quartz (SiO_2) and Na feldspar ($NaAlSi_3O_8$) grains ($\varnothing = 150$–250 μm) extracted from a sediment sample no. 972505. Each aliquot of Al_2O_3:C consisted of a single pellet, whereas each aliquot of quartz and Na feldspar consisted of about 500 grains. The OSL measurement protocol for Al_2O_3:C consisted of irradiation, preheat to 180 °C, cool down to room temperature, and OSL measurement at 30 °C for 500 s. For quartz and feldspars the preheat temperature was 260 °C (10 s) and 250 °C (60 s), respectively, and the OSL signal was corrected for sensitivity changes by using a test dose OSL signal with the same preheat [24].

3. Results

We first make a comparative examination of the OSL decay behaviour of Al_2O_3:C (TLD 500) after exposure to beta, proton and x-ray irradiation to understand the OSL response to x-rays. We then test this understanding with two other materials, namely quartz and Na feldspar.

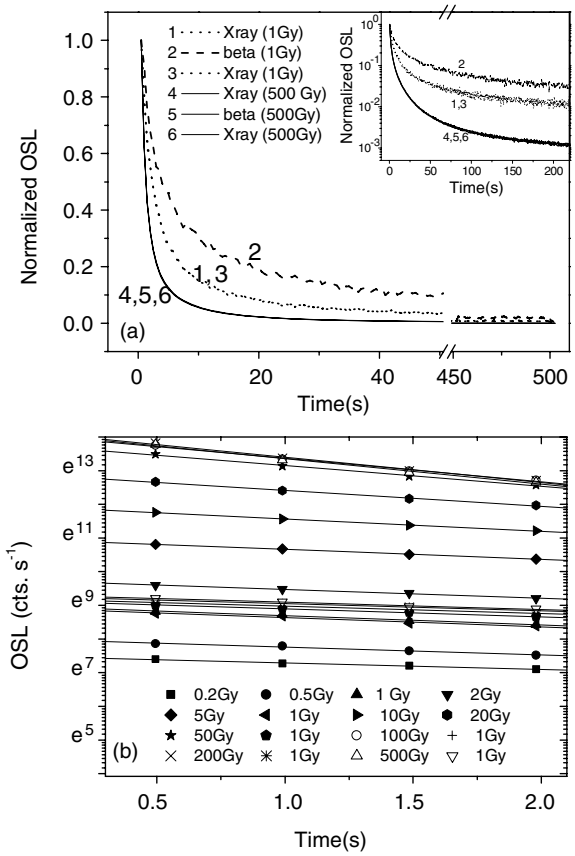

Figure 1. (a) OSL decay curves of Al_2O_3:C after beta and 50 kV x-ray irradiations. The inset shows the same data on a log OSL scale for the first 200 s of stimulation. The data are normalized with respect to the initial intensity in each OSL decay curve. Optical stimulation was carried out for 500 s at 30 °C after a preheat to 180 °C. (b) Fitting of an exponential decay equation ($L(t) = L_0 e^{-\lambda t}$) to the initial OSL obtained during the first 2 s for different doses. Note that OSL values are plotted on a ln axis. Each of the fits had R^2 value of better than 0.99.

3.1. Decay shape of the OSL signal from Al_2O_3:C

It has been shown qualitatively that the decay rate of the OSL signal from Al_2O_3:C increases with an increase in the absorbed dose from beta particles, and that the same effect is observed when heavy charged particles are used for irradiation [25–27]. This effect is analysed below to understand the dose deposition process for x-rays by comparing the OSL decay rates obtained after x-ray irradiation with those obtained after beta (^{90}Sr/^{90}Y) and proton irradiation.

3.1.1. OSL response to beta irradiation. An aliquot of Al_2O_3:C was sensitized by repeated irradiation of up to 2 kGy, preheat and OSL measurements. After this procedure the aliquot always produced the same OSL for a given dose irrespective of the previous dose and OSL history. A dose response curve was measured on this sensitized aliquot for different beta doses ranging from 200 mGy to 500 Gy. The normalized OSL decay curves obtained for doses after 1 and 500 Gy are shown in figure 1(a). The OSL signal decay after the 1 Gy dose (curve 2) is

much more rapid than after the 500 Gy dose (curve 5), which is in accordance with earlier work (see [27]). It is also observed that the OSL signal decays non-exponentially (figure 1(a) inset). This non-exponential decay shape has been suggested to arise from a non-first-order kinetic process [31, 32] or from a superimposition of several first-order OSL components [28–30]. A significant body of experimental work suggests that the main dosimetric thermoluminescence (TL) or thermally stimulated conductivity (TSC) peak in Al_2O_3:C is composed of several overlapping first-order peaks and that there is a relationship between these peaks and the OSL signal [30, 33, 34]. For example, the low temperature part of the 450 K TL peak is easily bleachable and thermal annealing of the low temperature part removes the fast decaying OSL component [33]. Investigations using optical conductivity and OSL measurements in Al_2O_3:C suggest that there exist several traps with different optical depths and photoionization cross-sections. During optical stimulation the charge decay from these individual traps follows first-order kinetics [28, 29]. Thus OSL signal can be resolved into about three first-order OSL components [30, 32] with cross-sections ranging from 3.3×10^{-20} to 1.5×10^{-18}.

In our OSL data the very beginning (∼2 s) of the OSL decay curve is well described by a single exponential of the form $L(t) = L_0 e^{-\lambda t}$ for all absorbed doses (figure 1(b)). Here L is the luminescence signal at stimulation time t and λ is the decay constant. Using this exponential function excellent fits were obtained for our data and values of λ derived for each OSL curve for each dose. The data were all collected with a constant flux of 1.06×10^{17} cm^{-2} s^{-1} of blue light (470±30 nm), and derived values of λ are only relevant for these experimental conditions. We emphasize that our exponential fit is a purely empirical representation of the initial decay rates of our curves; no assumption of physical process is implied (see section 3.1.5).

Six repeat OSL measurements of a 1 Gy dose were measured at different stages in the experiment (i.e. following OSL from 0.5, 5, 50, 100, 200 and 500 Gy) to check the reproducibility of our system (see repeat points in figure 2). The standard deviation on mean λ from these six repeat measurements was 4%, and it includes measurement and fitting uncertainties, as well as minor changes in the response of the dosimeter with repeated irradiation and OSL.

The data in figure 1(b) suggest that the initial OSL has a faster decay at higher doses. The decay constants (λ_i) for OSL obtained after different doses (D_i) are shown in figure 2(a). It is observed that the decay constant is ∼0.2 s^{-1} at a dose of 200 mGy and then increases as a function of beta dose to ∼0.8 s^{-1} at 250 Gy, after which it does not increase significantly.

This growth behaviour can be well described by a saturating exponential function of the form:

$$\lambda(D) = \lambda_0 + A(1 - e^{-b \cdot D}) \tag{1}$$

where λ_0 is the decay constant for an infinitesimally small dose, and b is a geometric constant that defines the curvature of the growth function. We discuss later (section 3.1.5) that λ_0 is a characteristic of the radiation's LET. For the beta irradiation it is calculated to be $\lambda_{0(\beta)} = 0.218 \pm 0.008$ s^{-1} by fitting equation (1) to the data in figure 2(a).

The OSL dose response function $L(D)$, which shows the variation in integral OSL signal intensity (for the first 50 s) as a function of dose is shown in figure 2(b). It is observed that the functional form of $L(D)$ is similar to that of $\lambda(D)$ (figure 2(a)), however, the dose at which saturation in the decay constants occurs (i.e. ∼100–250 Gy) is about five times the dose at which the saturation in the OSL response occurs (i.e. ∼20–50 Gy).

3.1.2. OSL response to proton irradiation. Different aliquots of Al_2O_3:C were irradiated with proton beams ranging from 60 to 11 MeV to obtain an absorbed dose of 5 Gy. This dose was

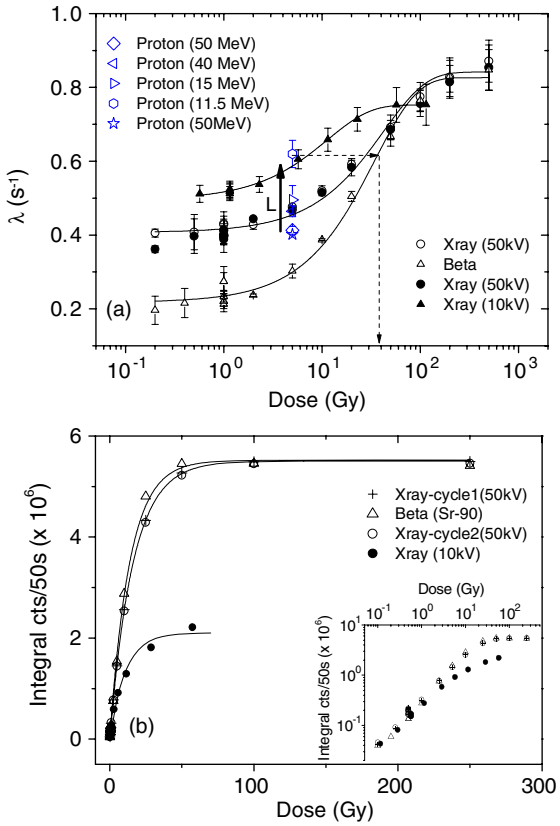

Figure 2. Initial OSL decay rate (λ) of Al_2O_3:C as a function of given dose for different kinds of radiations. (b) The OSL dose response of Al_2O_3:C for different radiation types. The net OSL signal was calculated using light integral in the first 50 s of the OSL decay curve after subtracting the background (average OSL in the 476–500 s interval). As observed in figure 1 inset the OSL signals drop by more than two orders of magnitude in the first 50 s of optical stimulation.

(This figure is in colour only in the electronic version)

monitored using an ionization chamber. The proton LET in Al_2O_3:C for these energies varies between 3.4 keV μm^{-1} (60 MeV) and 13.1 keV μm^{-1} (11 MeV). Three aliquots of Al_2O_3:C were irradiated for each proton energy. These aliquots were subsequently brought back to the laboratory and had their OSL measured. The OSL decay rate differs significantly from one aliquot to another because of slightly different defect concentrations, so it is difficult to directly compare the OSL decay rates for different proton energies using different aliquots. To overcome this problem the OSL decay rate for each proton irradiated aliquot was normalized by its OSL decay rate after a 5 Gy beta dose given in the laboratory. Subsequently, all these ratios were multiplied with the OSL decay rate of the Al_2O_3:C pellet used in section 3.1.1 after a 5 Gy beta dose.

It is observed that for the same absorbed dose the decay constant increases with the proton LET (solid arrow in figure 2(a)). The fact that the corrections involved in the decay constant calculation are acceptable is confirmed by similar decay constants obtained for two different aliquots that were exposed to 50 MeV protons.

3.1.3. OSL response to 50 kV x-ray irradiation. The same Al_2O_3:C pellet that was used in the beta dose response experiment (section 3.1.1) was exposed to 50 kV x-rays filtered through a 200 μm aluminium absorber. A dose response curve was measured (figure 2(b)). In order to check the reproducibility of our results, the 50 kV data set was re-measured after measuring the OSL dose response curve to beta radiation ranging from 200 mGy to 500 Gy. The two OSL decay curves and the dose response data measured for 50 kV x-ray are indistinguishable (see figures 1, 2(a) and (b)) suggesting a good reproducibility in our dosimeter and the overall measurement system.

The OSL signals obtained after the 1 Gy x-ray dose (curves 1 and 3 in figure 1) decay much more rapidly than those obtained after a 1 Gy beta dose (curve 2 in figure 1). However, the OSL decay curves after a 500 Gy x-ray dose (50 kV) are identical to those obtained after a 500 Gy beta dose (curves 4, 5 and 6 in figure 1). A summary of decay constants for various absorbed doses for the 50 kV x-ray is shown in figure 2(a). The fitting of the data with equation (1) gave $\lambda_0 = \lambda_{0(X-50)} = 0.401 \pm 0.006\ s^{-1}$. This shows that the λ_0 value for 50 kV x-rays is about 100% larger than that for beta irradiation ($\lambda_{0(\beta)} = 0.218 \pm 0.008\ s^{-1}$, section 3.1.1).

3.1.4. OSL response to 10 kV x-ray irradiation. The same Al_2O_3:C pellet as above was finally exposed to 10 kV x-rays and a dose response curve measured (figure 2(b)). The net OSL signal output at the saturation level is much lower for 10 kV irradiation than that after 50 kV x-ray or beta irradiation. We interpret this effect to arise because of the thickness of the sample; this gives rise to an overall reduction in the OSL output at the saturation level. The thickness of Al_2O_3:C pellet is about 1 mm. This thickness gives rise to existence of a dose gradient for both $^{90}Sr/^{90}Y$ beta and x-ray irradiations [35]. This dose gradient is expected to be significantly steeper for 10 kV x-rays than for 50 kV x-rays because of the energy difference. As long as there is no charge saturation effect in the traps (i.e. the linear region of the growth curve), the luminescence response of 10 kV x-rays will be similar to that from beta particles and 50 kV x-rays; this is because x-ray dose rate calibration is derived by matching luminescence response at low dose from beta particles (section 2). However, at higher doses the part of the crystal facing the irradiation source will begin to reach charge saturation faster for 10 kV x-ray compared to that for beta particles (or 50 kV x-rays); this occurs because of steeper dose gradient in the former case and will cause, on an average, an early saturation in the OSL response. Similarly the total OSL at saturation will depend on the total number of traps available; this will clearly be greater in the case of beta particles (or 50 kV x-rays) as compared to 10 kV x-rays since a larger volume of the crystal is accessible. Both these saturation behaviours can be observed for 10 kV x-rays in figure 2(b). By same reasoning a good agreement between the 50 kV x-ray and the beta dose response curves suggests that the two kinds of radiations produce similar dose gradients in the crystal.

Regarding the OSL decay rate response it can be observed that at low doses the OSL decay rate for 10 kV x-rays is higher than that for 50 kV x-rays (figure 2(a)). The data were again fitted to a saturating exponential dose response function (equation (1)) and a $\lambda_0 = \lambda_{0(X-10)} = 0.495 \pm 0.003\ s^{-1}$ was derived. This value is significantly greater than the values obtained for beta particles $\lambda_{0(\beta)}$ and 50 kV x-rays $\lambda_{0(X-50)}$.

3.1.5. Interpretation of the OSL decay response to beta particles, protons and x-rays. We discuss here the various OSL responses presented above to understand the dose deposition process by x-rays. An important observation is that there occurs an increase in the decay constant of the initial OSL with dose. Similar behaviour has been also seen in TL where the peak shifts to lower temperatures at higher doses. However the peak shift occurs in discrete

steps and cannot be explained by simple non-first-order processes; an overlap of first-order peaks is used to explain the effect [33]. Since it has been shown that the low temperature part of TL has higher photoionization cross-section [33], a peak shift to lower temperatures with dose would imply that the fast OSL component(s) is (are) growing more rapidly then the slower components. This would cause the overall OSL decay to be faster for higher absorbed doses [32].

It is interesting to note that the two dose responses, the net OSL $L(D)$ and its decay rate $\lambda(D)$, have similar functional forms. If the OSL curve is arising from superimposition of several first-order traps with different photoionization cross-sections then a saturation in $\lambda(D)$ could occur as the trap with the largest photoionization cross-section (but with an overall small contribution to the integral OSL used for dose response curve) begins to saturate with dose [28, 32].

The alternative possibility of non-first-order decay cannot be ruled out. The present data could also be related to the process of trap filling during irradiation—one for the dosimetric trap and another for a competing trap, and a subsequent competition process during the optical stimulation. Let us assume that the OSL decay is related to the rate of change of holes at the recombination centres $(-\mathrm{d}m/\mathrm{d}t)$. These holes will have slower depletion if another light sensitive trap competes for charge evicted from the main dosimetric trap during the optical stimulation. The extent of this competition will depend upon how many sites of the competing trap are unoccupied and hence available for the competition. Since the competing trap would have filled up in a saturating exponential manner with prior dose, it is expected that the competition offered by it will decrease exponentially with dose towards the state in which almost no competition occurs. In other words the decay constants will increase exponentially towards a value that is possible when all the competing traps are full[2]. This will cause $\lambda(D)$ to have a saturating exponential form described by equation (1). The same results could also be achieved with only one trap, one recombination centre model if there is significant retrapping during optical stimulation. This has been shown to be the case when the probability of retrapping is close to that of recombination [32].

The above discussion implies that the decay constant λ, derived from the initial OSL signal only, cannot be directly attributed to the actual detrapping probability ξ ($\xi_i = \sigma_i \cdot \phi$, photoionization cross-section for each trap times the photon flux) of any of the participating traps. It is in fact an apparent decay constant, perhaps, arising either from superimposition of several first-order OSL components [28–30, 32] responding differently to dose, or from the non-first-order kinetics. Both these mechanisms cause λ to vary as a function of dose (discussed in section 3.1.5).

The constant offset $\lambda_0 = \lambda_{0(\beta)}$ in the in $\lambda(D)$ function for the beta particles is the smallest decay constant achievable by an infinitesimally small dose. In the case of beta particles, which is a low LET radiation, the irradiation is microscopically uniform[3]. Therefore, a small given dose gives rise to a relatively small microscopic dose as well. However, for high LET radiations,

[2] In a first-order case of electron capture during irradiation the rate of change of the number of electrons in the competing trap follows $-\mathrm{d}n/\mathrm{d}D \propto (N - n)$, which can be solved to $N - n = N \cdot \mathrm{e}^{-b \cdot D}$. Here N and n are the concentrations of competing traps and trapped electrons, respectively, b is a constant, and $N - n$ defines the concentration of sites available for competition after the irradiation. The OSL signal $(-\mathrm{d}m/\mathrm{d}t)$ then arises from competition from N traps at zero dose, assuming that all the traps were empty at the beginning of irradiation, and $N - n$ traps at dose D. At a high dose $N - n \approx 0$; hence there are no sites available for competition and, therefore, the change in the $-\mathrm{d}m/\mathrm{d}t$ will be the maximum. For intermediate doses λ will increase as a saturating exponential function since $N - n$ decays exponentially.

[3] This is because beta particles do not follow a straight path, and further that the stopping power of the primary particles ($\overline{E} \approx 600$ keV) is 1.6 MeV cm^2 g^{-1}, which is an order of magnitude smaller compared to the stopping power of say 10 MeV protons (=35.43 MeV cm^2 g^{-1}) in aluminium oxide.

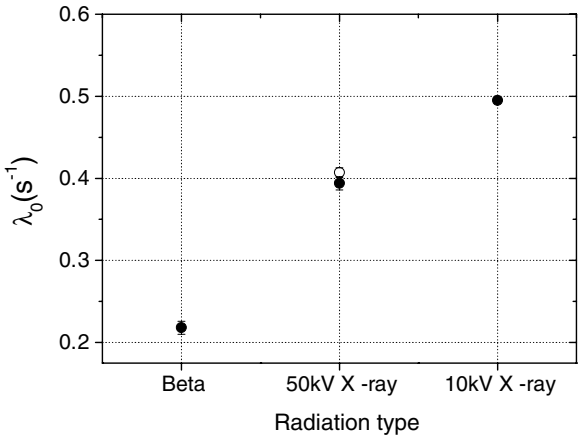

Figure 3. A plot of λ_0 values for different kinds of radiations. These values are determined by fitting a saturating exponential + a constant (λ_0) function (equation (1)) to the data in figure 2(a). The unfilled circle shows the reproducibility of the λ_0 value obtained using repeat measurements of the OSL response to 50 kV irradiations (see section 3.1.3 for details).

e.g. protons, a small absorbed dose can results in a large microscopic dose because of the high ionization density around the proton track. The λ_0 value will, therefore, be smaller for beta particles than for protons since even for an infinitesimally small dose the fast decaying trap (or the competing trap) will be relatively closer to saturation due to the higher ionization density in the latter case. This implies that the main control on the OSL decay rate is the spatial distribution of dose. Since λ_0 is controlled by the extent of ionization density (per particle) even at infinitely small doses, it can be argued that the λ_0 value will be a characteristic of the LET of the radiation. The same applies to the OSL decay rate λ. Note, for example, that the decay constant obtained after 5 Gy dose from 11 MeV protons is comparable to that obtained after a 40 Gy beta dose (dashed arrow in figure 2(a)). This suggests that, as far as the OSL traps are concerned, the 5 Gy dose with 11 MeV protons is on an average effectively equivalent to about 40 Gy if the sample were to be irradiated uniformly.

On the basis of the above reasoning we conclude that a relatively higher OSL decay rate of Al_2O_3:C after a given dose (below 50 Gy) of x-rays compared to that after the same dose of beta particles (figure 2(a)) suggests a higher ionization density and charge saturation effect associated with x-rays. This results in an increasing trend in the OSL decay rate for a given dose ($\lambda_\beta < \lambda_{X-50} < \lambda_{X-10}$) before saturation, as well as in a systematic increase in the λ_0 values ($\lambda_{0(\beta)} < \lambda_{0(X-50)} < \lambda_{0(X-10)}$) (figure 3). Thus, the ionization density for 10 kV x-rays is inferred to be greater than that for 50 kV x-rays which in turn is greater than that for beta particles.

The inference obtained above of high ionization density and local saturation effects associated with low energy x-rays would imply that the OSL response to x-rays would strongly depend on the concentrations of traps and/or centres that take part in the luminescence process and their capture cross-sections. This would cause the OSL response to x-ray irradiation to be material dependent. The OSL saturation behaviour with dose can be determined using beta and gamma radiations since the sample is irradiated uniformly with these low LET radiations. In the following section we test whether the local saturation effect explanation based on the OSL decay shape of Al_2O_3:C can explain the material specific OSL response to x-rays observed by Thomsen *et al* [10] and Jain *et al* [12].

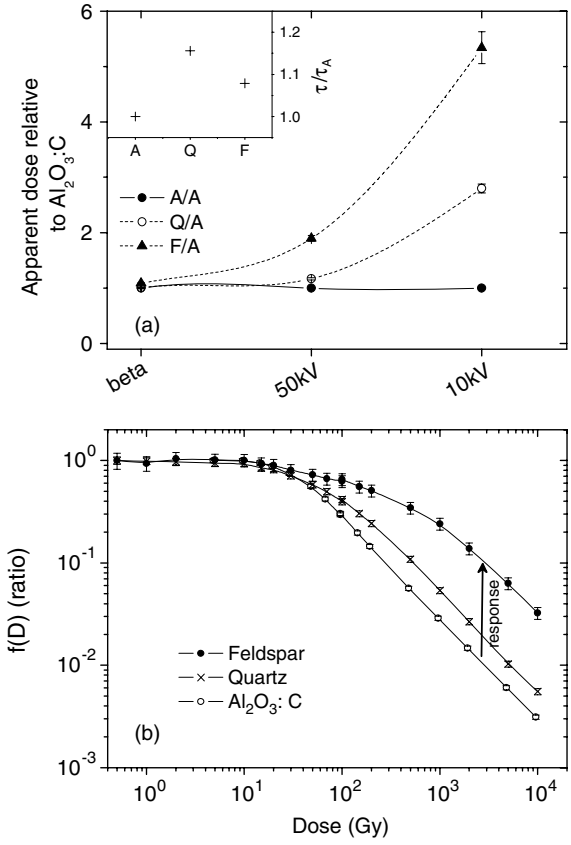

Figure 4. (a) Apparent dose calculated using OSL signal from quartz, feldspars or Al_2O_3:C (normalized with respect to that from Al_2O_3:C) for the same given duration of irradiation to each materials. The apparent dose values were calculated for beta particles, 50 kV x-rays and 10 kV x-rays. The absolute reference in these calculations is a 5 Gy gamma dose from ^{137}Cs source (see the text for details). The inset shows the photo electric cross-sections for the three materials normalized by the cross-section value for Al_2O_3:C. (b) The OSL response function $f(D)$ measured using dose from ^{90}Sr/^{90}Y beta particles in quartz, feldspar and Al_2O_3:C.

3.2. Testing the 'ionization density effect' model in OSL from other dosimeters

OSL responses of quartz, feldspars and aluminium oxide. The samples of quartz grains (Q), feldspar grains (F) and Al_2O_3:C (A) were given a dose of 5 Gy using a ^{137}Cs point source. The three samples were then preheated and the gamma induced OSL signal measured and corrected for sensitivity change. Each samples was then irradiated with ^{90}Sr/^{90}Y beta particles, 50 kV x-rays or 10 kV x-rays for the measurement of sensitivity-corrected OSL dose–response curve for each radiation type [24]. The gamma induced OSL signals were interpolated on these OSL response curves to determine the equivalent irradiation time for beta source and the x-rays. An apparent dose rate for each radiation type in each material is calculated by dividing the known ^{137}Cs dose of 5 Gy with the equivalent irradiation time for each of the radiation type. The apparent dose rate data for each material and radiation was finally normalized with the dose rate for Al_2O_3:C for the same radiation. The data in this form represent a relative dose (with respect to that for Al_2O_3:C) that would be measured for each material if they were exposed to the same type of radiation for the same period of time. These data are plotted in figure 4(a)

as a function of radiation type for the three materials. It is observed that for 50 kV x-rays the apparent doses in quartz and feldspar are ∼1.1 and 1.9 times of that for Al_2O_3:C, respectively. And for 10 kV x-rays the apparent dose in quartz and feldspar are ∼3 and ∼5 times that in Al_2O_3:C. This suggests the both quartz and feldspar samples investigated here have an over response compared to Al_2O_3:C.

At these low x-ray energies the main mode of energy loss is photoelectric absorption so it can be argued that the above behaviour may be caused by the differences in the photoelectric cross-sections in these materials. These differences in cross-sections can result in different absorbed doses for the same radiation exposure time. The inset in figure 4(a) shows the relative photoelectric absorption coefficient (τ/τ_A = ratio of the cube of the effective Z values) of each material with respect to that of Al_2O_3:C. The differences in the τ/τ_A values for these materials is less than 20% ($A < F < Q$) and is not in the same order as that observed in the apparent dose data ($A < Q < F$). Therefore the difference in τ values does not explain the observed differences in the apparent dose.

However, the observed material dependence may be explained by the ionization density effects as inferred in section 3.1 for x-rays. For low energy photons (50 and 10 kV x-rays) the OSL response will depend on local charge saturation effects because of high ionization density; this will result in a change in OSL efficiency[4]. The extent of efficiency change will be related to the saturation behaviour of OSL traps with dose. Since beta particles irradiate the sample uniformly they can be used to quantify the OSL saturation behaviour with dose. Figure 4(b) shows the response function $f(D)$ for each material given by:

$$f(D) = \frac{L/D}{L_l/D_l} \tag{2}$$

where L is the measure of luminescence signal after a given dose D, and L_l and D_l are any corresponding luminescence and dose values in the linear region of the growth curve. For a typical saturating exponential OSL dose response function, the $f(D)$ will be unity up to a certain dose and then decrease with a further increase in the dose. This function represents how efficient a certain dose is in producing luminescence [31] and as can be seen in figure 4(b) the efficiency drastically decreases with an increase in dose because of the reduction in the available traps or centres.

The luminescence response trends in figure 4(b) show that at high doses the efficiency is maximum for feldspars followed by quartz and finally Al_2O_3:C ($F > Q > A$) (see the arrow in figure 4(b)). From a microscopic dose deposition point of view, we would expect that for the same absorbed x-ray dose the OSL efficiency (and hence the apparent dose measured using OSL) of these materials will also follow the above trend; this is because of the high ionization density and charge saturation effect during x-ray interaction. This is indeed the case (figure 4(a)). Thus the data from low LET irradiation (beta particles) support our hypothesis of high local ionization density effect in x-ray irradiation based on the changes in the initial OSL decay rate in Al_2O_3:C. It also suggests that this effect is the main reason for the material dependent dose rate values observed in different materials by Jain *et al* [12], and that the differences in photoionization cross-sections are irrelevant for these materials. It must, however, be cautioned that large differences in sample responses observed for 10 kV x-rays (3–5 times, figure 4(a)) must partly be produced because of the differences in the thickness of quartz and feldspar samples compared to that of the Al_2O_3:C pellet (section 3.1.4). For 50 kV x-rays, this difference is negligible because of a good agreement in the OSL dose response curves for beta and 50 kV x-ray irradiations (figure 2(b)) for Al_2O_3:C (the thickest dosimeter).

[4] Efficiency is the ratio between the luminescence response to a small dose from a given type of radiation and the luminescence response to the same dose with a low LET radiation such as ^{137}Cs gamma rays.

4. Potential use of Al_2O_3:C for radiation of unknown LET

We discuss in section 3.1.5 that the decay constant of the initial OSL after an infinitely small dose (λ_0) is a characteristic of the (apparent) LET of an ionizing radiation. λ_0 shows a systematic increase with the apparent LET, for example $\lambda_{0(\beta)} < \lambda_{0(X-50)} < \lambda_{0(X-10)}$ (figure 3). Further it is shown in figure 2(a) and equation (1) that the exact form of the variation in λ with dose is unique for the three radiation types (beta, 50 kV x-rays and 10 kV x-rays), and it is argued that this function depends upon the (apparent) LET of the radiation. Both these properties of Al_2O_3:C can be used to quantify the LET of the radiation and hence the absorbed dose using OSL.

For example consider a case in which it is desirable to measure the dose deposited by a proton beam at a fixed point in a phantom. As the proton beam passes through the phantom there is a change in its energy and thereby its LET. This makes it difficult to measure dose deposited using an OSL dosimeter since the LET of the proton at the target and the corresponding OSL efficiency are unknown.

If the mean energy of the incident beam is kept the same then the OSL decay rate can be used to decipher the LET and hence dose at the target. To achieve this, the OSL decay curve after an infinitesimally small duration of proton exposure at the target is measured. This decay rate corresponds to λ_0. Since λ_0 is expected to be unique for each proton LET (L), it should match one of the values from the known $\lambda_0(L)$ values for the dosimeter. LET corresponding to the observed match will be the LET of the radiation at the target. And the efficiency[4] value for this LET can be used to determine the true dose rate.

Alternatively, the OSL response and its decay constant (λ) can be measured as a function of the duration of the radiation exposure (t) which should follow (see section 3):

$$\lambda(t) = \lambda_L + A(1 - e^{-b \cdot t}) \tag{3}$$

where λ_L is the decay constant offset in the dose response curve (equation (1)) corresponding to the LET (L) of the proton or any other radiation. The radiation duration (t) can be converted to dose (D in equation (1)) if the true dose rate can be calculated. In order to determine the dose rate one can use the expected proton LET at the target as the input parameter to calculate the OSL efficiency from a known efficiency versus LET function for protons. On the basis of the efficiency value the corresponding dose rate can be calculated. The LET value is then varied and the process iterated until a unique match is obtained between the data (equation (3)) and the known $\lambda(D)$ function for a particular proton LET for the dosimeter. Since the function is unique for a particle's LET there will only be one match. Also the dose rate corresponding to this match will be the true luminescence dose rate and hence a correct estimate of dose at the target can be calculated.

5. Summary and discussion

We have shown that the initial OSL decay rate (λ) in Al_2O_3:C increases as a function of dose for a given ionizing radiation. This work is in agreement with the study by Yukihara *et al* [27] using beta particles. We further show that the $\lambda(D)$ function has a well defined form of a saturating exponential with a constant offset λ_0. This functional relationship can be explained by either a superimposition of first-order OSL components saturating at different rates with dose, or a charge capture by a competing trap during optical stimulation. We also observe an increase in the OSL decay rate when protons of different energies are used to deposit a 5 Gy dose.

Previous studies using thermoluminescence from lithium fluoride (LiF) dosimeters have shown that the TL sensitivity is a function of x-ray energy below 100 keV; the TL efficiency

variations are up to 30% [13, 16]. Such data are explained using various microdosimetric models [14, 19]. The response of the OSL signal to x-rays has not been previously investigated. We show here that the shape of the OSL decay curve from Al_2O_3:C (TLD 500) [22] directly records the presence of a high ionization density (apparent LET effect) in low energy x-ray irradiation. There occurs a systematic increase in the initial OSL decay rate, $\lambda_{\text{beta}} < \lambda_{50\text{ kV}} < \lambda_{10\text{ kV}}$ and the respective λ_0 values because of an increased microscopic deposition of dose (figure 2(a)). The magnitude of the change in the initial OSL decay constant (λ) is more than 100% when 50 and 10 kV x-rays are compared to low LET beta particle (^{90}Sr/^{90}Y). This change is about three to four times higher than the previously reported effect of low energy x-ray irradiation on the TL efficiency of LiF of ∼30%. These microdosimetric effects occur because the electron energy spectrum produced by such low energy x-rays interactions has a higher average stopping power as compared to that produced by high energy photon interactions [36]. For example, the average stopping power of an electron spectrum produced by 3, 15 and 662 keV photon interaction in water is 76.7, 27.8 and 3.47 MeV cm^2 g^{-1}, respectively (table A-3b in Johns and Cunningham [37]). The above mechanism of localized dose deposition explains both the problem of material dependent calibration and that of sample dependent calibration in x-ray radiation, reported in other studies [10, 12].

Finally we argue that the λ_0 value and the $\lambda(D)$ function (saturating exponential + a constant) are unique for a radiation's LET (figures 2(a), 3). We define these for beta particles and 50 and 10 kV x-rays for our dosimeter and stimulation flux. These results suggest that the greater the LET (or apparent LET) of the radiation the greater the λ_0 value. It may be possible to use these characteristics to quantify the LET of a radiation where it cannot be measured directly, e.g. charged particle therapy.

The comparison of the $\lambda(D)$ function for x-rays with that for beta particles depends on the accuracy of the dose rate calibration for x-rays. The x-ray dose rates were derived by matching the OSL response after a low dose, D, (in the linear region of the growth curve) from ^{90}Sr/^{90}Y beta irradiation with that after x-ray. The derived x-ray dose rates for each material can only be considered approximate since there will be efficiency differences between x-rays and beta particles. Nonetheless, a good agreement between the OSL dose response curves for beta and 50 kV x-rays (figure 2(b)) suggests that the calculated dose rates are acceptable. Moreover, the dose rates for 50 and 10 kV x-rays were also measured with a radiation sensitive film (gafchromatic EDT dosimetric film) and these were in good agreement with those derived using the OSL of Al_2O_3. Efficiency variations of up to 30% have been suggested by other workers for LiF [13, 14, 16, 18]. The efficiency values for Al_2O_3:C may be close, however, even in the worst case scenario, if our dose rate values were to be off by a factor of two (i.e. scaling the dose axis for x-rays in figure 2(a) by a factor of 2) the initial OSL decay constants after x-ray irradiation will still be significantly higher than those after beta irradiation. Thus the interpretations presented here will still be valid.

6. Conclusions

We give evidence for high local ionization density in 50 and 10 kV x-ray excitations using luminescence based detection of trapped charge in carbon doped aluminium oxide (Al_2O_3:C). This effect is similar to that produced by high LET radiations such as protons. These results are a first account of ionization density and local saturation effect in OSL produced by x-rays in natural and synthetic materials.

We show that in Al_2O_3:C the nature of increase in the OSL decay constant (for initial signal) with dose, $\lambda(D)$, has a form of a saturating exponential with a constant offset (λ_0). Both $\lambda(D)$ and λ_0 are unique for a given radiation type, or more specifically its LET. Below

the saturation dose, the $\lambda_{\text{beta}} < \lambda_{50\text{ kV}} < \lambda_{10\text{ kV}}$ and $\lambda_{0(\beta)} < \lambda_{0(X-50)} < \lambda_{0(X-10)}$. This systematic increase in the initial OSL decay rate occurs because of charge saturation effect in the OSL traps due to high local ionization density (microscopic dose) during x-ray interaction. This high ionization density results from low energy electrons produced mainly from direct photoelectric absorption.

We suggest that the OSL decay rate of Al_2O_3:C is a powerful tool to look into the ionization density phenomenon caused by x-rays because of high sensitivity of λ to the microscopic dose. We show an increase in λ of more than 100% when, for example, 10 kV x-rays are compared with ^{90}Sr/^{90}Y beta particles. This approach of using λ may be more robust than that based on changes in TL or OSL sensitivity since luminescence sensitivity variations are small (up to 30%) and can depend on several factors, e.g. the previous dose and heating history of the sample.

Finally, we demonstrate that the x-ray dose calibration problem in different materials can be explained by the apparent LET effect (high ionization density) for low energy x-rays.

Acknowledgments

This is a contribution to European Space Agency project ESTEC, Contract no. 18581/04/NL/HB. We are grateful to the two anonymous referees for their detailed, constructive comments.

References

[1] Aznar M C, Hemdal B, Medin J, Marckmann C J, Andersen C E, Bøtter-Jensen L, Andersson I and Mattsson S 2005 *Br. J. Radiol.* **78** 328–34
[2] Gaza R, McKeever S W S, Akselrod M S, Akselrod A, Underwood T, Yoder C, Andersen C E, Aznar M C, Marckmann C J, Bøtter-Jensen L, Nikl M, Bos A J J, Tale I, Fabeni P, Nitsch K and Mihokova E 2004 *Radiat. Meas.* **38** 809–12
[3] Alonso P J, Halliburton L E, Kohnke E E and Bossoli R B 1983 *J. Appl. Phys.* **54** 5369–75
[4] Halliburton L E 1989 *Appl. Radiat. Isot.* **40** 859–63
[5] Marazuev Yu A, Brik A B and Degoda V Ya 1995 *Radiat. Meas.* **24** 565–9
[6] Halperin A and Sukov E W 1993 *J. Phys. Chem. Solids* **54** 43–50
[7] Bisello D, Candelori A, Kaminski A and Litovchenko A 2004 *Radiat. Phys. Chem.* **71** 713–5
[8] Andersen C E, Bøtter-Jensen L and Murray A S 2003 *Radiat. Meas.* **37** 557–61
[9] Hong D G, Kim M J, Yawata T and Hashimoto T 2005 *J. Radioanal. Nucl. Chem.* **265** 495–8
[10] Thomsen K J, Bøtter-Jensen L, Denby P M and Murray A S 2006 *Nucl. Instrum. Methods Phys. Res.* B **252** 267–75
[11] McKeever S W S, Banerjee D, Blair M, Clifford S M, Clowdsley M S, Kim S S, Lamothe M, Lepper K, Leuschen M, McKeever K J, Prather M, Rowland A, Reust D, Sears D W G and Wilson J W 2003 *Radiat. Meas.* **37** 527–34
[12] Jain M, Andersen C E, Bøtter-Jensen L, Murray A S, Haack H and Bridges J C 2006 *Radiat. Meas.* **41** 755–61
[13] Budd T, Marshall M, Peaple L H J and Douglas J A 1979 *Phys. Med. Biol.* **24** 71–80
[14] Horowitz Y and Olko P 2004 *Radiat. Prot. Dosim.* **109** 331–48
[15] Harris C K, Elson H R, Lamba M A S and Foster A E 1997 *Med. Phys.* **24** 1527–9
[16] Olko P, Bilski P and Kim J L 2002 *Radiat. Prot. Dosim.* **100** 119–22
[17] Horowitz Y S 1981 *Phys. Med. Biol.* **26** 765–824
[18] Olko P, Bilski P, Budzanowski M, Waligorski M P R, Fasso A and Ipe N 1999 *Radiat. Prot. Dosim.* **84** 103–8
[19] Olko P, Bilski P, Budzanowski M, Waligorski M P R and Reitz G 2002 *J. Radiat. Res.* **43** S59–62
[20] Geiß O B, Kramer M and Kraft G 1998 *Nucl. Instrum. Methods Phys. Res.* B **142** 592–8
[21] McKeever S W S, Blair M W, Bulur E, Gaza R, Gaza R, Kalchgruber R, Klein D M and Yukihara E G 2004 *Radiat. Prot. Dosim.* **109** 269–76
[22] Akselrod M S, Kortov V S, Kravetsky D J and Gotlib V I 1990 *Radiat. Prot. Dosim.* **33** 119–22
[23] Bøtter-Jensen L, Andersen C E, Duller G A T and Murray A S 2003 *Radiat. Meas.* **37** 535–41
[24] Murray A S and Wintle A G 2000 *Radiat. Meas.* **32** 57–73
[25] Yasuda H and Kobayashi I 2001 *Radiat. Prot. Dosim.* **95** 339–43

[26] Yasuda H, Kobayashi I and Morishima H 2002 *J. Nucl. Sci. Technol.* **39** 211–3
[27] Yukihara E G, Gaza R, McKeever S W S and Soares C G 2004 *Radiat. Meas.* **38** 59–70
[28] Whitley V H and McKeever S W S 2000 *J. Appl. Phys.* **87** 249–56
[29] Whitley V H and McKeever S W S 2001 *J. Appl. Phys.* **90** 6073–83
[30] Whitley V H and McKeever S W S 2002 *Radiat. Prot. Dosim.* **100** 61–6
[31] Chen R and McKeever S W S 1997 *Theory of Thermoluminescence and Related Phenomenon* (Singapore: World Scientific)
[32] Yukihara E G, Whitley V H, McKeever S W S, Akselrod A E and Akselrod M S 2004 *Radiat. Meas.* **38** 317–30
[33] Akselrod A E and Akselrod M S 2002 *Radiat. Prot. Dosim.* **100** 217–20
[34] Agersnap Larsen N, Bøtter-Jensen L and McKeever S W S 1999 *Radiat. Prot. Dosim.* **84** 87–90
[35] Greilich S and Andersen C E 2006 Calibration of thick dosimeters using β, γ and x-rays *UK Luminescence and ESR Mtg (Liverpool)* (Abstract)
[36] Sugiyama H 1985 *Phys. Med. Biol.* **30** 331–5
[37] Johns H E and Cunningham J R 1983 *The Physics of Radiology* (Springfield, IL: Charlie Thomas)